ANNALS OF GEOPHYSICS, 65, 4, GD430, 2022; doi:10.4401/ag-8770
OPEN ACCESS

Seismic assessment of high-rise buildings through dynamic nonlinear analysis

Xiuwen Wu[1] and Daoyun Lin[*,2]

(1) Hainan Hongjing Architectural Design Co., Ltd., Haikou, China
(2) Dowsion Science and Technology Engineering (Hainan) Co., Ltd., Haikou, China

Article history: received December 1, 2021; accepted May, 2, 2022

Abstract

This paper present a seismic assessment of high-rise buildings using dynamic nonlinear analysis. The work touches upon an urgent problem of ensuring the stability of high-rise buildings under seismic load and preventing their destruction. A mathematical model has been built to investigate the effect of seismic activity on high-rise buildings in the Sichuan province (China). Pearson's test was used to compare the statistical dependence between variables in the study period. Values with a statistical significance of $p \leq 0.05$ were considered statistically significant. The probability of earthquakes of 8 magnitude and above was found to be 5% with a frequency of recurrence of 3900 ± 400 yrs, $p \leq 0.001$. The paper presents the technique of refractive geophysical research. The seismic reliability index was $n = 3.2$ at $t = 5$ s. The standard deviation was 2% and the χ^2 statistic was 0.95. The overall (0.59, or 59%) and conditional (0.06, or 6%) risks of failure under seismic load were calculated for high-rise buildings with a service life of 100 years. The coefficients of seismic activity were as follows: 3.203 at the conditional risk level of 5%; 2.97 at the conditional risk level of 10%; and 2.523 at the conditional risk level of 30%.

Keywords: High-rise building; Incremental dynamic analysis; Seismic force; Soil; Structure reliability.

1. Introduction

Seismic and paraseismic tremor shocks represent a type of dynamic load. The seismic-type shocks are associated with earthquakes, the natural, short-term shaking of the ground caused by the propagation of seismic waves through the depths of the Earth. Earthquakes can be divided into three categories based on depth of the shaking: shallow, intermediate, and deep. Seismic tremors are of three types: tectonic (the most common one), volcanic, and collapse. They are characterized by these estimates: the total radiated energy, E (J); the maximum acceleration, a_{max} (cm/s^2); radius of action, r (km); the size of the area under risk, A (km^2); and the number of protrusions. Paraseismic tremors results human activities, such as mining, mine or quarry blasting, pile driving activity (in close proximity of the building), and vibrations generated by industrial equipment and vehicles. The most common cause of paraseismic tremors is mining, but they also can be produced by heavy traffic in large cities. Mining tremors can be seen in previously exploited areas many years after exploitation because of disturbances in the geostatic

balance of rock mass that the exploitation process causes. Moreover, scientists highlight a continuous increase in the intensity of these tremors, in China specifically [Tan et al., 2020; Kumar et al., 2021].

When planning the construction multi-storey buildings in an area with increased seismic activity, project managers have to establish seismic risks and failure criteria. One reason behind vibrations is unbalance [Sheng et al., 2020]. In this case, it is best to balance the moving masses. This strategy for vibration reduction is also applied to equipment and different mechanisms, especially their rotary and reciprocating parts. One type of unbalance is a displacement of the gravity center of a load rotating around the eccentric, an unbalance which increases the centrifugal force [An et al., 2021]. To prevent this, one can reduce the amplitude by balancing the mass of the movement so that the rotating mass is close to the axis of rotation of the mass [Li, 2021]. The eccentricity is this case does not matter. This solution was employed in some skyscraper constructions [Al-Kodmany, 2014; Contin, 2021]. There are more reasons for unwanted vibration, which are associated with equipment aging and malfunction [Beketaeva et al., 2016]. Therefore, it is important to keep an eye on the state of machinery in order to immediately alleviate all defects and visible signs of wear [Kapasakalis et al., 2021]. Thin-walled building structures (such as chimneys) can develop vibrations under the action of air flow. To mitigate the effects of aerodynamic forces on buildings, a special construction device is used, which can resemble a turbo isolator [Huo et al., 2021]. Architecture engineering under earthquake conditions is a subject of attention, which is considered by all participants in the construction project, especially in earthquake-prone regions [Sheng et al., 2020].

In China, such region make up more than 25% of the country's land. The skyscraper construction projects in the country have recently moved to seismic zones, which were previously poorly populated and not used for permanent construction purposes [Jiang et al., 2020]. Potentially, these zones can be used to build industrial enterprises, residential complexes, and other structures. Yet, given the risk of paraseismic events in the area of high-rise building construction, the structural reliability of the buildings should be significantly improved [Lei et al., 2020].

According to seismologists and eyewitnesses, the seismic activity has two distinct phases: (1) the short phase, which lasts a total of several seconds, sometimes preceded by smaller foreshocks [Oliveira and Correia, 2021]; and (2) the subsequent phase, sometimes followed by aftershocks (rocks destruction during the movement of tectonic platforms) [Liu and Zahradník, 2020]. The short phase of the shock occurs due to crushing of the rock mass in places of concentration of forces that shift geologic platforms of the earth's crust. The subsequent phase (oscillations with gradual attenuation) follows a shift of the foundation of the structure. Sometimes the frequencies of natural vibrations are close to or even coincide with the frequencies of forced vibrations. In this case, vibration of the buildings increases [Wang and Huang, 2020]. This can be avoided by changing the vibration frequency of the system itself. For this, the value of the vibrating mass or stiffness of the system must be corrected [Xu et al., 2020]. Another way is to use special mufflers that help to damp vibration [Kaczmarczyk, 2021]. These devices are commonly employed in the construction of tall, slender buildings and are part of a special assembly [Bollano et al., 2021]. Nonlinear dynamic analysis methods are used to study earthquakes and predict the extent of destruction [Forcellini, 2019]. This technique is widely used not only in China (Sichuan Province, Qinghai Province, Yunnan Province, etc.), but also in Italy, Japan, the Philippines, Singapore and many other countries [Chen, et al. 2021; Bollano et al., 2021]. Destruction of structures usually occurs under the action of the first shock. It can be due to the impact action of soil on the structure, which results in stress that arises within the structure and leads to cracking and failure. If the building did not collapse during the first (short) phase, then the damage is likely repairable [Dalle et al., 2021; Wang and Shen, 2020]. Therefore, when designing a building, it is very important to estimate the level of stress from the shock during its short phase in order to ensure the strength of the structure [Qingyun et al., 2021]. The present work aims to conduct a series of numerical tests to determine the sensitivity of nonlinear dynamic systems to seismic conditions.

2. Materials and methods

2.1 Study location

The study was conducted in Sichuan province, China, a region which has small (ML <5) but frequent earthquakes. Normally, these are earthquakes that follow a major tectonic element – a southwest (SW) trending anticline. An anticline is a system of nappes/folds (3-6 km thick) that slowly slide along the underlying base [Liu and Zahradník, 2020].

2.2 Refraction technique

A refraction technique utilizes the 'sliding' of waves along the boundaries of layers with different wave velocities. This phenomenon is characterized by an increase in velocity with depth. Due to this feature, this geophysical method is suitable for the accurate recognition of boundaries. A seismic refraction analysis reveals deep sections with marked layers and changes in wave velocity. Using refraction techniques allows a quasi-continuous representation of the structure of the center with accuracy unattainable in geotechnical engineering.

2.3 Statistical analysis

Statistical data processing was performed using Pearson's chi-squared (χ^2) test and t-test. Pearson's test was used to compare the statistical dependence between variables in the study period. The 95% confidence interval has been determined. Statistical significance was set at $P < 0.005$. Standard deviation and variance were also determined. All calculations were performed in MS Excell and Statistica.

2.4 Mathematical modeling of seismic shock based on the shockwave theory

The velocity of seismic compression (σ) and shear (τ) waves propagating through different materials (soil and concrete) after shock depends on the elastic properties of those materials, such as elastic modulus (E) and density (ρ). The vibration velocity of particles in the wave front was designated as V.

Note that the process of wave transmission usually occurs amid the continuous interaction between soil and foundation (before destruction). Hence, the above properties can all be considered in the context of continuity. In addition to that, the impact energy from the earthquake is continuously converted to deformation energy of the medium proportionally to its modulus of elasticity. Such representation of the soil-foundation interaction process allows calculating the relationship between soil V_S and concrete V_b velocities of vibration for particles in the compression and/or shear wave fronts. This enables the calculation of the normal compressive stress (σ_b) and shear stress (τ_b) acting on concrete [Li and Su, 2021; Wang et al., 2021b].

Penetration of shock waves into a building/structure occurs in two ways: through the lateral surface and through the foundation of the construction at the points of contact with the ground (Figure 1). Due to the impact action of soil on the lateral surface of the foundation, waves propagating through the body of the foundation will create normal stress (σ). Equations describing the continuity of wave-front stress and velocity at the interface between the soil (σ_s) and the lateral vertical face of the foundation (σ_1) can be expressed as follows:

$$\sigma_s + \Delta\sigma_s = \sigma_b \tag{1}$$

$$V_S + \Delta V_S = V_b \tag{2}$$

The proportional relationship between the relative deformation and the ratio of soil and concrete velocities can be determined using the following equation:

$$\sigma_b = \varepsilon E_b = \frac{V_b}{V_\sigma^b} E_b \tag{3}$$

In a similar way to equation (3), we wrote

$$\sigma_s = \frac{V_s E_s}{V_\sigma^s} \tag{4}$$

$$\Delta\sigma_s = \frac{\Delta V_s E_s}{V_\sigma^s} \tag{5}$$

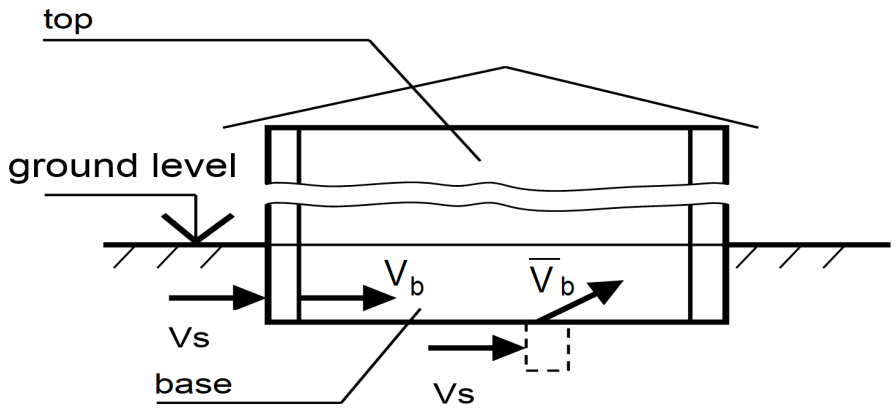

Figure 1. A schematic representation of shock waves propagating into a building.

Through the substitution of equation (5) to equation (1) and with due consideration to equation (4), we get:

$$\frac{V_s E_s}{V_\sigma^s} + \frac{\Delta V_s E_s}{V_\sigma^s} = \sigma_b \tag{6}$$

from which

$$\Delta V_s = \left(\sigma_b - \frac{V_s E_s}{V_\sigma^s}\right)\frac{V_\sigma^s}{E_s} \tag{7}$$

If we substitute equations (7) and (2) and transform the resulting formula, we will get:

$$\Delta V_s = V_s\left(1 + \frac{E_b}{V_\sigma^b}\frac{V_\sigma^s}{E_s}\right) \tag{8}$$

$$V_s = \frac{\Delta V_s}{1 + \frac{E_b}{V_\sigma^b}\frac{V_\sigma^s}{E_s}} \tag{9}$$

The shockwave theory holds that the velocity of shock wave propagation in different materials (V_σ^b, V_τ^b, V_σ^s, and V_τ^s) depends on deformation modules (E and G) and density (ρ) of the material. For concrete, it is equal to:

$$V_\sigma^b\sqrt{\frac{E_b}{\rho_b}}V_\tau^b = \sqrt{\frac{G_b}{\rho_b}} \tag{10}$$

For soil, it will be:

$$V_\sigma^s\sqrt{\frac{E_s}{\rho_s}}V_\tau^s = \sqrt{\frac{G_s}{\rho_s}} \tag{11}$$

If we express the concrete and soil velocities of compression waves in terms the properties these two media have, the equation (9) will be written as follows:

$$V_b = \frac{\Delta V_s}{1+\sqrt{\frac{E_b\rho_b}{\rho_s E_s}}} \tag{12}$$

The second way of impact energy propagation is through the base of the foundation, where the transfer of energy occurs under the action of shear stress (τ_S) at the soil-foundation contact. Continuity equations for wave velocity (V_S) and shear stress at the soil-foundation interface can be expressed in a similar way to equations (13) and (14):

$$\tau_s + \Delta\tau_s = \tau_b \tag{13}$$

$$V_S + \Delta V_S = \overline{V}_b \tag{14}$$

The proportional relationship between the relative deformation and the ratio of soil and concrete velocities during shear can be expressed as:

$$\tau_s = \frac{V_s G_s}{V_\tau^s} \tag{15}$$

$$\Delta\tau_s = \frac{\Delta V_s G_s}{V_\tau^s} \tag{16}$$

The stress, in this case, will depend on the adhesion of soil to the foundation, which is characterized by the coefficient of adhesion (C). The values of τ_S and $\Delta\tau_S$ must be adjusted to the ratio between the adhesion coefficient and its largest value, which is equal to the shear strength of the medium (soil or concrete). Normally, this property is taken as $(1.5 \div 2.5)R_{bt}$ but this study assumes that it is equal to. In a similar way to equation (7), we thus get:

$$\Delta V_s = \left(\tau_b - V_s \frac{G_s}{V_\sigma^s}\right)\frac{V_\sigma^s}{G_s}\frac{R_{bt}}{C} \tag{17}$$

Substituting equations (17) and (15) to equation (14) gives:

$$\overline{V}_b = \left(\frac{1+\frac{R_{bt}}{C}}{1+\frac{R_{bt}}{C}\frac{G_b V_s}{G_\tau^b G_s}}\right) \tag{18}$$

and if we consider equations (10) and (11), the final formula will be:

$$\overline{V}_b = \frac{\left(1+\frac{R_{bt}}{C}\right)V_s}{1+\frac{R_{bt}}{C}\sqrt{\frac{G_b\rho_b}{G_s\rho_s}}} \tag{19}$$

Besides shear stress, transmission of impact energy can cause normal stress on structure's foundation, which will complement normal stress from shock waves that hit the side surface of the building. The shear stress, which results from the force acting on the lateral surface of the foundations can arise in the superstructure at the edge of the foundation and combine with shear stress produced during the transmission of impact energy through the bottom part of the foundation. The superstructure stress can thus be determined using combined velocity (V_Σ), the formula of which is:

$$V_\Sigma = V_b + \overline{V}_b \tag{20}$$

When planning the construction of the underground part of the building, stress values should be computed by the following formula:

$$\sigma_b = \sigma(V_b) + \sigma\left(\overline{V}_b\right) \tag{21}$$

In formulas (1) to (21) above, the following designations are used:

V_S, V_b, and $\overline{V}_b$ are the compressional wave-front velocities of horizontal displacement in the soil medium, under the transmission of impact energy through the foundation's lateral surface, and under the transmission of impact energy through the bottom part of the foundation, respectively;

ΔV_S, ΔV_b, and $\Delta\overline{V}_b$ represent the increment of horizontal velocities at the interface of two media on impact;

V_σ^b, V_τ^b, and V_σ^s represent the velocities of waves (compressional and shear) propagating within the soil medium and concrete medium, which depend on the elastic properties of those media;

σ_s, σ_b, and $\tau_b$are the compressive stress and the tangential (shear) stress on the soil and concrete;

$\Delta\sigma_s$, $\Delta\sigma_b$, and $\Delta\tau_b$ represent increments of stress at the interface of two media;

E_S, E_b, G_b, and G_b are deformation moduli and shear moduli of soil and concrete;

ρ_s and ρ_b represent the densities of soil and concrete, respectively.

The velocity (V_S) of horizontal movement of the soil can be determined by the following formula:

$$V_s = \gamma \cdot t \tag{22}$$

where: γ is the acceleration of ground movement during an earthquake and t is the duration of the impulse of the force.

Based on international standards [Wang et al., 2021a], the numerical values of ground surface acceleration (γ) were established with regard to the magnitude of an earthquake. These values were expressed in millimeters per second (mm/s^2). The impact duration, however, is not normalized in terms of magnitude; therefore, it should be taken based on the results of seismogram analysis. To ensure reliability in calculations, the duration of shock should be taken in the range from 0.25 to 3 seconds, as suggested in literature [Sheng et al., 2020; An et al., 2021; Kumar et al., 2021].

According to the shockwave theory, the velocity (V) of horizontal displacement in the shock front can help to determine the magnitude of compressive and/or shear stress on a structure:

$$\sigma_{sp} = V\sqrt{\rho E} \tag{23}$$

$$\tau_{sp} = V\sqrt{\rho G} \tag{24}$$

When estimating the stress, a building/structure was considered as a complex isotropic system, although it is, in fact, an anisotropic system – a set of structural elements (such as walls, pillars, and floors). Stress values can vary from structure to structure (element to element). To consider this feature during calculations, the following equilibrium condition was employed:

$$\sigma_{sp}^{t.c\sum F_{t.c.}} = \sigma_{sp}^{p.c.\sum F_{p.c.}} \tag{25}$$

where: $\sigma_{sp}^{t.c\sum F_{t.c.}}$ and $\sigma_{sp}^{p.c.\sum F_{p.c.}}$ represent stress at the interface of shock-transmitting structures and shock-absorbing structures, respectively; $\sum F_{t.c.}$ and $\sum F_{p.c.}$ are the combined areas of cross-sections, which transmit and absorb the shock, respectively.

Based on equilibrium condition, stress on the shock-absorbing sections can be determined by this formula:

$$\sigma_{sp}^{p.c.} = \sigma_{sp}^{t.c.} \frac{\sum F_{t.c.}}{\sum F_{p.c.}} = \sigma_{sp}^{t.c.} K_t \tag{26}$$

where: K_t is a coefficient of transition, which takes into account the change in the magnitude of stress at the interface of structures with different areas.

The shear stress (τ) can be determined in a similar way:

$$\tau_{sp}^{p.c.} = \tau_{sp}^{t.c.} \frac{\sum F_{t.c.}}{\sum F_{p.c.}} = \tau_{sp}^{t.c.} K_t \tag{27}$$

Due to the fact that the shock wave propagating through the building's structures encounters resistance, it loses energy and gets extinguished. In other words, the horizontal displacement will decrease, resulting in the reduction of stress. Since the propagation of stress waves is similar to that of sound waves, one can assume that the decay of stress waves and sound waves occurs in the same way, that is, proportionally to the square of the travel distance. The loss of impact energy during the upward movement of a shock wave along the walls of a building, which attenuates at its top completely, can be taken into account by introducing the coefficient of attenuation to the stress value:

$$K_d = 1 - \left(\frac{h_i}{H}\right) \tag{28}$$

where: H is the height of a building, m; and h_i is the height at which the stress is computed.

Consequently, equations for stress on the upper structures from a shock wave produced by an earthquake are as follows:

$$\sigma_{sp}^{p.c.} = \sigma_{sp}^{t.c.} K_t K_d \tag{29}$$

$$\tau_{sp}^{p.c.} = \tau_{sp}^{t.c.} K_t K_d \tag{30}$$

When estimating stress on flat structures (such as floors), it is necessary to consider dissipation of energy in the horizontal direction due to deformation processes, as shown in Figure 2.

Under a linear law of stress reduction within half the span, the coefficient of dissipation for formulas (29) and (30) will be equal to 0.5.

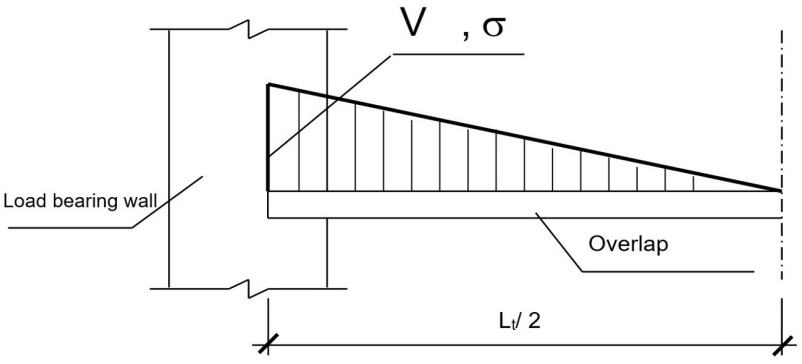

Figure 2. A representation illustrating energy dissipation of the ceiling.

3. Results

Since real-life systems are classified as nonlinear systems, the maximum value of the standard deviation is taken as $\sigma = 0.15$ m. To simplify the calculations, the examined system was linearized and considered as a quasilinear system. The dynamic intensity of the shock wave was calculated according to Rice's formula:

$$U(t) = T(t)\left(-\frac{\sigma 2_{ymax}}{2D_y(t)}\right) \tag{31}$$

where: $T(t)$ is the value of the effective period at time t, 1/s; σ_{ymax} is the maximum standard deviation; and $D_y(t)$ represents variance. A conditional risk of destruction ($H(t)$) was determined by using the following formula:

$$H(t) = 1 - exp\left(-\int_0^t U(t)dt\right) \tag{32}$$

The results from solving equations (31) and (32) are depicted in Figures 3 and 4, respectively.

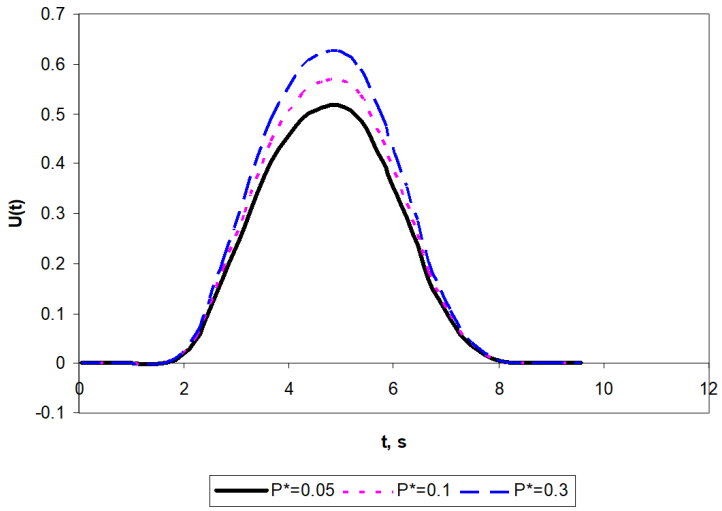

Figure 3. Shock-wave intensity $U(t)$ against time t.

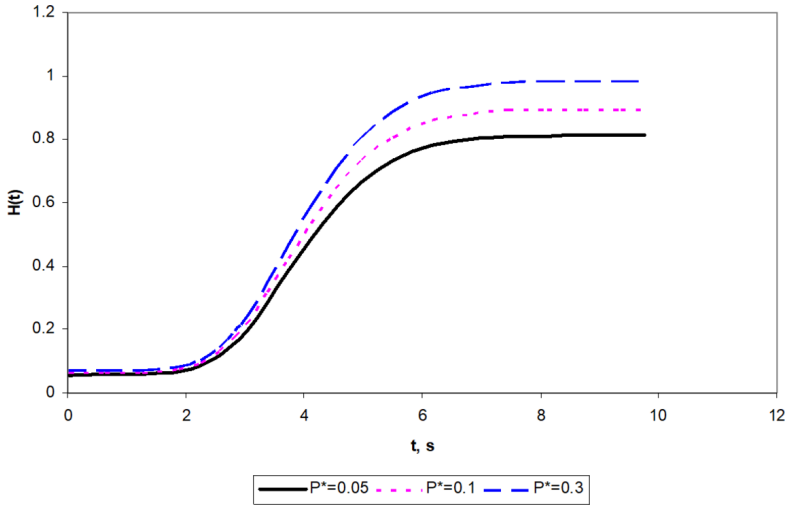

Figure 4. Conditional destruction risk curve.

When calculating the total risk of failure of the system, consideration was given to the estimate of seismic hazard of the territory, which obeys the Poisson's law:

$$H(t) = [1 - exp(-\Delta T)] \tag{33}$$

Note that there the intensity of seismic activity is likely to exceed the set level at least once. The overall probability of failure under seismic load is determined by this formula:

$$P(t) = 1 - exp\left(-\int_0^t U(t)dt\right)[1 - exp(-\Delta T)] \tag{34}$$

Theoretically, in the Sichuan province, the probability of earthquakes of 8 magnitude and above is 5% with a frequency of recurrence of 3900 ± 400 yrs, $p \leq 0.001$. The results of the reliability assessment of buildings, the service life of which is projected to be 100 years, are presented in Table 1.

Variable	Point of Time						
	0	1	2	4	6	8	10
Intensity, $U(t)$	0	0.003	0.028	0.525	0.377	0.025	0.011
Conditional probability of failure, $H(t)$	0	0.005	0.015	0.59	0.825	0.831	0.833
Overall probability of failure, $P(t)$	0	0	0.002	0.067	0.088	0.08	0.079

Table 1. Seismic reliability of a building at different points of time, s.

The results suggest that the study area is subjected to a substantial seismic risk, which is determined by the likelihood of damage to buildings. The conditional probability of failure of a building at the time a standard is reached was up to 59%. At the same time, the overall probability of failure was 6.7%. The seismic reliability index was calculated using this formula:

$$n = \sqrt{-2\,ln\left[-\frac{T_e\,ln(1-P^*)}{\tau}\right]} \tag{35}$$

where: T_e is the effective period of the system, 1/s; P^* is the conditional risk level (for the Sichuan province, it is equal to 0.05); and τ is the duration of the seismic activity. The theoretical value of the seismic reliability index was 3.2 at time t = 5 s with the standard deviation of 2% (Figure 5).

Conditional accelerations for a given frequency of the carrier wave($\omega(t)$) were calculated using this equation:

$$a^*(\tau) = \omega_m^2(t)\sigma_y(t) \tag{36}$$

The maximum shock-wave acceleration at time t = 5 s was $a^* = 4.195$ m/s. Under these conditions, the amplification factor was equal to 5.147. The probability of failure of a building was 59% with the maximum theoretical acceleration of the shock wave of 2.8%.

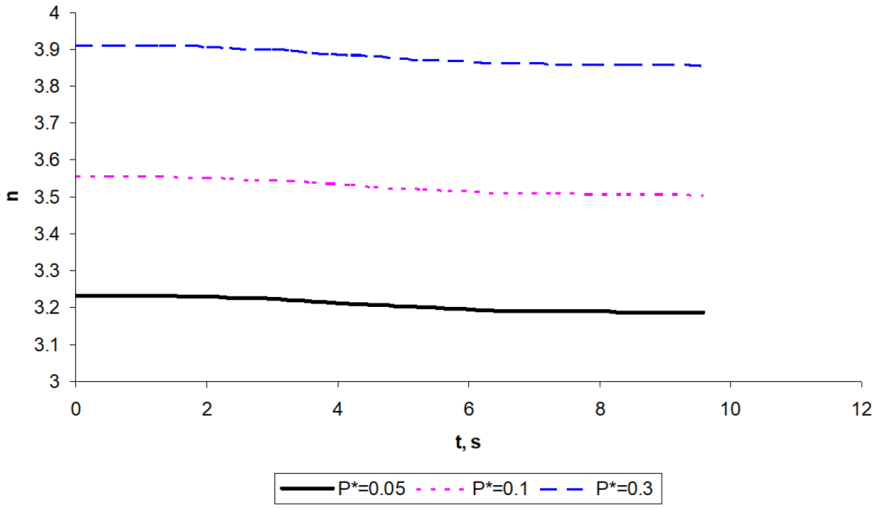

Figure 5. Changes over time in the seismic reliability of a building at the conditional risk level of $P^* = 0.05$; $P^* = 0.1$ and $P^* = 0.3$.

4. Discussion

The problem of seismic activity is important for many countries in the world. In particular, strong earthquakes occur in Italy, Indonesia, Japan, Armenia, etc. The use of seismic risk prediction models is important for such areas. The use of such techniques is quite common in worldwide practice [Contin, (2021); Kumar et al., 2021]. The results of this study show that in order to achieve the probability of system failure of 5%, the seismic load should be increased by 3.03 times. At the same time, a 30% failure probability is associated with the ultimate value of seismic load should be increased by 2.526 times. These findings coincide with previous research [Bollano et al., 2021].

The present calculations show that high-rise buildings are more likely to collapse during the oscillatory phase of an earthquake. According to the literature evidence, however, theoretical stress on loaded structures is greater than that from vibrations. Therefore, it is possible that results from the standard calculation can be lower than those from the strength calculations [Muscolino et al., 2021]. At the moment, there are no documents standardizing the conditional risk of destruction for high-rise buildings under seismic conditions; therefore, there is a substantial variation in its value between countries [Sabadash et al., 2020]. In this study, the conditional risk value was equal to 0.05.

The present results suggest that a building may fail either on the first impact or afterwards, during the subsequent oscillatory period. To avoid this, recommendations are given on strengthening or replacing the weak structures. Investigating the impact of kinematic excitation on the wall of a three-dimensional building [Taraszkiewicz et al., 2021], researchers carried out a series of numerical tests, which made it possible to determine the sensitivity of nonlinear dynamic systems to changes in properties of the medium and density of discretization, obtained with the finite element method (FEM). The study was performed on a 2D model of a frame-and-panel wall and a 3D model of a low-rise building, which were exposed to loads (kinematic input data) at time intervals consistent with earthquake accelerograms. The construction materials (masonry and concrete) were described using the Barcelona plastic damage model [Taraszkiewicz et al., 2021]. The advantage of this model is that it allows depicting the real properties of geomaterials, as well as considering material failure under cyclic loading. The disadvantage of this model is that when applied to integrate motion equations, it requires more computational studies, as the density of discretization, obtained with FEM, can affect the accuracy of a solution.

5. Conclusions

This paper presents a strategy for the probabilistic seismic (or paraseismic) performance assessment of high-rise buildings. The linearization of the mathematical model was performed with the help of canonical expansions. The results of seismic load modeling are presented as amplitude-frequency characteristics. The nonlinear system was characterized using a function of spectral frequencies and dynamic characteristics of the system. The max-

imum value of the amplification factor (at time t = 5 s) was 5.147. The values of these variables were adequate: standard deviation, SSE = 0.5; variance, 0.25; significance level, $p \leq 0.05$; and χ^2, 0.08. The characteristics of the system, presented as components of a quasilinear system, suggest that it the examined system is a 'narrow-band filter'. The results of the analytical calculation revealed the maximum displacement of 0.144 m at t = 5 s. Statistical analysis showed the standard deviation of 0.01% and the Student's t-statistic of 0.95.

References

Al-Kodmany, K. (2014). Green retrofitting skyscrapers: a review, Buildings, 4, 4, 683-710.

An, M., F. Zhang, E. Dontsov, D. Elsworth, H. Zhu and L. Zhao (2021). Stress perturbation caused by multistage hydraulic fracturing: implications for deep fault reactivation, Int. J. Rock Mech. Mining Sci., 141, 104704.

Beketaeva, A. O., Ye. S. Moisseyeva and A. Zh. Naimanova (2016). Numerical simulations of shock-wave interaction with a boundary layer in the plane supersonic flows with jet injection, Thermophys. Aeromechanics, 23, 2, 173-183.

Bollano, P. O. N., K. A. Kapasakalis, E. J. Sapountzakis and I. A. Antoniadis (2021). Design and optimization of the KDamper concept for seismic protection of bridges, in Proceedings of the 14th International Conference on Vibration Problems, Springer, Singapore, 193-215.

Chen, G., B. Ruan, K. Zhao, W. Chen, H. Zhuang, X. Du, and C. H. Juang (2020). Nonlinear response characteristics of undersea shield tunnel subjected to strong earthquake motions, J. Earthq. Eng., 24, 3, 351-380.

Contin, A. (2021). Metropolitan architecture 39, in Training for Education, Learning and Leadership Towards a New Metropolitan Discipline, A. Contin, P. Giordano and M. Nacke (Editors), CIPPEC, 56-76.

Dalle, J., P. Chetthamrongchai, G. Widjaja, E. Dudukalov, A. H. Iswanto and E. S. Sergushina (2021). Route optimization of container ships using differential evolution and gray wolf optimization, Ind. Eng. Manag. Syst., 20, 4, 604-612.

Forcellini, D. (2019). Numerical simulations of liquefaction on an ordinary building during Italian (20 May 2012) earthquake, Bull. Earthq. Eng., 17, 9, 4797-4823.

Huo, Y., W. Zhang and J. Zhang (2021). Centroid moment tensor of the 2019 MW 5.7 changning earthquake refined using 3d green's functions considering surface topography, Front Earth Sci., 9, 642721.

Jiang, D., S. Zhang and R. Ding (2020). Surface deformation and tectonic background of the 2019 Ms 6.0 Changning earthquake, Sichuan basin, SW China, J. Asian Earth Sci., 200, 104493.

Kaczmarczyk, S. (2021). The dynamic interactions and control of long slender continua and discrete inertial components in vertical transportation systems, in Nonlinear Dynamics of Discrete and Continuous Systems, Springer, Cham, 117-128.

Kapasakalis, K. A., I. A. Antoniadis and E. J. Sapountzakis (2021). KDamper concept for base isolation and damping of high-rise building structures, in Proceedings of the 14th International Conference on Vibration Problems, Springer, Singapore, 265-289.

Kumar, T., R. Kumar and S. C. Jain (2021). Numerical investigation of semi-active torsional vibration control of heavy turbo-generator rotor using magnetorheological fluid dampers, J. Vib. Eng. Technol., in press.

Lei, X., J. Su and Z. Wang (2020). Growing seismicity in the Sichuan Basin and its association with industrial activities, Sci. China Earth Sci., 63, 1633-1660.

Li, C. and L. Su (2021). Influence of critical acceleration model on assessments of potential earthquake-induced landslide hazards in Shimian County, Sichuan Province, China, Landslides, 18, 5, 1659-1674.

Li, J. (2021). Vibration response test method of curtain wall under seismic coupling, Arab. J. Geosci., 14, 6, 1-9.

Liu, J. and J. Zahradník (2020). The 2019 MW 5.7 Changning earthquake, Sichuan Basin, China: A shallow doublet with different faulting styles, Geophys. Res. Lett., 47, 4, e2019GL085408.

Muscolino, G., F. Genovese, G. Biondi and E. Cascone (2021). Generation of fully non-stationary random processes consistent with target seismic accelerograms, Soil Dyn. Earthq. Eng., 141, 106467.

Oliveira, C. S. and P. Correia (2021). Comparison of the seismic and wind analyses of two tower cranes, J. Vibroengineering, 23, 4, 1-20.

Qingyun, D., T. Fei, S. Yanhui, G. Rui, L. Sanzhong, F. Changmin, W. Guangzeng, L. Feng and T. Yuyang (2021). Linkage of deep lithospheric structures to intraplate earthquakes: a perspective from multi-source and multi-scale geophysical data in the South China Block, Earth Sci. Rev., 214, 103504.

Sabadash, V., J. Gumnitsky and O. Lyuta (2020). Combined adsorption of the copper and chromium cations by clinoptilolite of the Sokyrnytsya deposit, J. Ecol. Eng., 21, 5, 42-46.

Sheng, M., R. Chu, S. Ni, Y. Wang, L. Jiang and H. Yang (2020). Source parameters of three moderate size earthquakes in Weiyuan, China, and their relations to shale gas hydraulic fracturing, J. Geophys. Res. Solid Earth., 125, 10, e2020JB019932.

Tan, Y., J. Hu, H. Zhang, Y. Chen, J. Qian, Q. Wang, H. Zha, P. Tang and Z. Nie (2020). Hydraulic fracturing induced seismicity in the southern Sichuan Basin due to fluid diffusion inferred from seismic and injection data analysis, Geophys. Res. Lett., 47, 4, e2019GL084885.

Taraszkiewicz, A., K. Grębowski, K. Taraszkiewicz and J. Przewłócki (2021). Medieval bourgeois tenement houses as an archetype for contemporary architectural and construction solutions: The example of historic downtown Gdańsk, Buildings, 11, 3, 80.

Wang, H. and Z. Huang (2020). Seismic tomography in the southern margin of the Sichuan Basin: Insight into the plateau-craton interaction and seismotectonics in the SE Tibetan Plateau, J. Asian Earth Sci., 199, 104464.

Wang J., X. Shen, Y. Yang, Z. Zeren, G. Hulot, N. Olsen, B. Zhou, W. Magnes, A. De Santis, J. P. Huang, F. Guo, W. L. Liu and J. B. Yu (2021a). Initial scalar lithospheric magnetic anomaly map of China and surrounding regions derived from CSES satellite data, Sci. China Technol. Sci., 64, 9, 1118-1126.

Wang M. and Z. K. Shen (2020). Present-day crustal deformation of continental China derived from GPS and its tectonic implications, J. Geophys. Res. Solid Earth., 125, 2, e2019JB018774.

Wang, X. Q., J. Wei, J. K. Zhao, Z. Zhou and Z. Huang (2021b). Simulation of the dynamic disturbance characteristics of the soft sediment in the Diexi ancient dammed lake, China, J. Mt. Sci., 18, 4, 990-1002.

Xu, L., Y. Cui and Z. Wang (2020). Active tuned mass damper based vibration control for seismic excited adjacent buildings under actuator saturation, Soil Dyn. Earthq. Eng., 135, 106181.

***CORRESPONDING AUTHOR: Daoyun LIN**,
Dowsion Science and Technology Engineering (Hainan) Co., Ltd., Haikou, China,
email: daoyunlin@yahoo.com